

AQC systems. They are scalable, easily manipulated, and have perfectly acceptable decoherence times, and no existing technological barriers seem to be present.

References and Notes

1. R. P. Feynman, in *Feynman Lectures on Computation*, A. J. G. Hey and R. W. Allen, Eds. (Addison-Wesley, Reading, MA, 1997), chap. 6.
2. S. Lloyd, *Sci. Am.* **273**, 140 (October 1995).
3. J. Preskill, *Proc. R. Soc. London Ser. A* **454**, 385 (1998).
4. P. W. Shor, *Proceedings of the 35th Annual Symposium*

Foundations of Computer Science, S. Goldwaser, Ed. (IEEE Computer Society, Los Alamitos, CA, 1994), pp. 124–134.

5. L. K. Grover, *Phys. Rev. Lett.* **79**, 325 (1997).
6. J. I. Cirac and P. Zoller, *ibid.* **74**, 4091 (1995).
7. Q. A. C. Turchette, C. J. Hood, W. Lange, H. Mabuchi, H. J. Kimbel, *ibid.* **75**, 4710 (1995).
8. S. A. Lloyd, *Science* **261**, 1569 (1993).
9. D. Loss and D. P. DiVincenzo, *Phys. Rev. A* **57**, 120 (1998).
10. B. E. Kane, *Nature* **393**, 133 (1998).
11. E. Y. Andrei, Ed., *Two Dimensional Electron Systems on Helium and Other Cryogenic Substrates* (Academic Press, New York, 1991).
12. C. C. Grimes et al., *Phys. Rev. B* **13**, 140 (1976).

13. K. Shirahama et al., *J. Low Temp. Phys.* **101**, 439 (1995).
14. L. D. Landau and E. M. Lifschitz, *Quantum Mechanics (Non-Relativistic Theory)* (Pergamon, Elmsford, NY, ed. 3, 1977), p. 145.
15. C. C. Grimes and G. Adams, *Phys. Rev. Lett.* **42**, 795 (1979).
16. M. I. Dykman, *Phys. Status Solidi B* **88**, 463 (1978).
17. G. Saville, J. Goodkind, P. M. Platzman, *Phys. Rev. Lett.* **70**, 1517 (1993).
18. We thank M. Lea, P. Fozoni, A. Dahm, and J. Goodkind for agreeing to actually launch experiments on such systems. We would also like to acknowledge many discussions with A. Mills about quantum computing.

17 February 1999; accepted 10 May 1999

Spontaneous Bubble Domain Formation in a Layered Ferromagnetic Crystal

T. Fukumura,^{1*} H. Sugawara,^{1†} T. Hasegawa,² K. Tanaka,^{3‡} H. Sakaki,^{3§} T. Kimura,⁴ Y. Tokura^{4,5}

Magnetic domain structure on the surface of the layer-structured ferromagnet La_{1.4}Sr_{1.6}Mn₂O₇ was observed in the temperature range from 37 to 97 kelvin with a scanning Hall probe microscope. The sensitivity to temperature of the domain structure changes was large relative to that in conventional ferromagnets. The stable and spontaneous appearance of magnetic bubble domains without an external magnetic field was observed in the neighborhood of 70 kelvin. The phenomenon observed could provide a potential route toward magnetic bubble memory.

The development of the computer industry demands higher density magnetic recording memory, which is being achieved by using smaller magnetic domains. The bubble domain is considered useful as a magnetic bit of high-density magnetic recording memory, because its diameter is small and the circular shape of the bubble domain is stable against any small external disturbance that deforms it (1). However, the bubble domain is not widely used for recording memory because the generation of a magnetic do-

main requires an external magnetic field. The minimization of the sum of the domain wall energy and the magnetostatic energy results in the appearance of a stripe domain instead of a bubble domain unless a magnetic field is applied (2). This stripe domain is not completely satisfactory for high-density recording.

We observed a domain structure along the surface of the single crystal of a layered ferromagnetic material, La_{1.4}Sr_{1.6}Mn₂O₇, with a scanning Hall probe microscope (SHPM). The domain structure was remarkably different from that of conventional bulk ferromagnetic materials. Small bubble domains formed in the absence of an external magnetic field over a certain temperature range.

Single crystals of La_{1.4}Sr_{1.6}Mn₂O₇ were grown by the float-zone method (3). This compound has a naturally built-in ferromagnetic multilayer structure regarded as an infinite stacking of magnetic (MnO₂ bilayer) and nonmagnetic layers [(La, Sr)₂O₂ layer] and exhibits a marked change in its magnetic structure with temperature (4, 5). Recent muon spin rotation (6) and neutron diffraction measurements (7) have revealed that long-range ferromagnetic coupling within a bilayer evolves below ~90 K, where the magnetic moments begin to rotate toward the *c* axis (perpendicular to MnO₂ bilayers) with decreasing tempera-

ture. At temperatures below 60 K, the magnetic moments of respective single MnO₂ layers couple ferromagnetically within a bilayer and align nearly along the *c* axis. The magnetic coupling between the adjacent MnO₂ bilayers is mostly antiferromagnetic.

The cleaved *ab* plane (parallel to MnO₂ bilayers) of a single crystalline platelet sample (2 mm by 1.4 mm by 0.8 mm) was examined under a homemade variable-temperature SHPM (8). The SHPM is designed to pick up the spatial distribution of the magnetic field just above the sample surface by scanning a horizontally placed miniature Hall probe. The distribution of the *c*-axis component of the magnetic field, *B_c*, was imaged by keeping a probe-to-sample distance of ~0.5 μm. The active area of the Hall probe was 1.8 μm by 1.8 μm, and its Hall coefficient was ~1.2 ohm/mT. Under a zero magnetic field, the SHPM measurements were performed from 37 to 97 K. The Hall probe was scanned over the same area throughout the measurements, although the scanned area became narrower as the temperature was lowered because of the reduction of the piezoelectric constant. SHPM images were taken at various temperatures (Fig. 1).

At 37 K, the observed *B_c* was approximately zero over most of the scanned area (Fig. 1A), representing the disappearance of net magnetization due to antiferromagnetic coupling between adjacent MnO₂ bilayers; that is, the magnetization of the adjacent bilayers is opposite each other, yielding zero magnetic field above the sample surface. However, magnetic domains were observed on the right-hand side of the image. At 51 K, these ferromagnetic domains occupied nearly half of the imaged area (Fig. 1C). As temperature was increased, the area of the domains expanded, accompanied by the increase in *B_c*. These images (Fig. 1, A to C) indicate the existence of ferromagnetic coupling between the adjacent MnO₂ bilayers, as well as the antiferromagnetic coupling.

At 60 K, a multidomain structure appeared throughout the imaged area with a domain size of ~3 μm (Fig. 1D). The domains had an elongated shape and were ar-

¹Department of Applied Chemistry, University of Tokyo, Tokyo 113-8656, Japan. ²Materials and Structures Laboratory, Tokyo Institute of Technology, Yokohama 226-8503, Japan. ³Research Center for Advanced Science and Technology, University of Tokyo, Tokyo 153-8904, Japan. ⁴Joint Research Center for Atom Technology, Tsukuba 305-0046, Japan. ⁵Department of Applied Physics, University of Tokyo, Tokyo 113-8656, Japan.

*To whom correspondence should be addressed. Present address: Department of Innovative and Engineered Materials, Tokyo Institute of Technology, Yokohama 226-8502, Japan. E-mail: fukumura@oxide.rlem.titech.ac.jp

†Present address: Department of Electronic Systems Engineering, Tokyo Metropolitan Institute of Technology, Tokyo 191-0065, Japan.

‡Present address: Department of Physical Electronics, Hiroshima University, Higashihiroshima 739-8526, Japan.

§Present address: Institute of Industrial Science, University of Tokyo, Tokyo 106-8558, Japan.

REPORTS

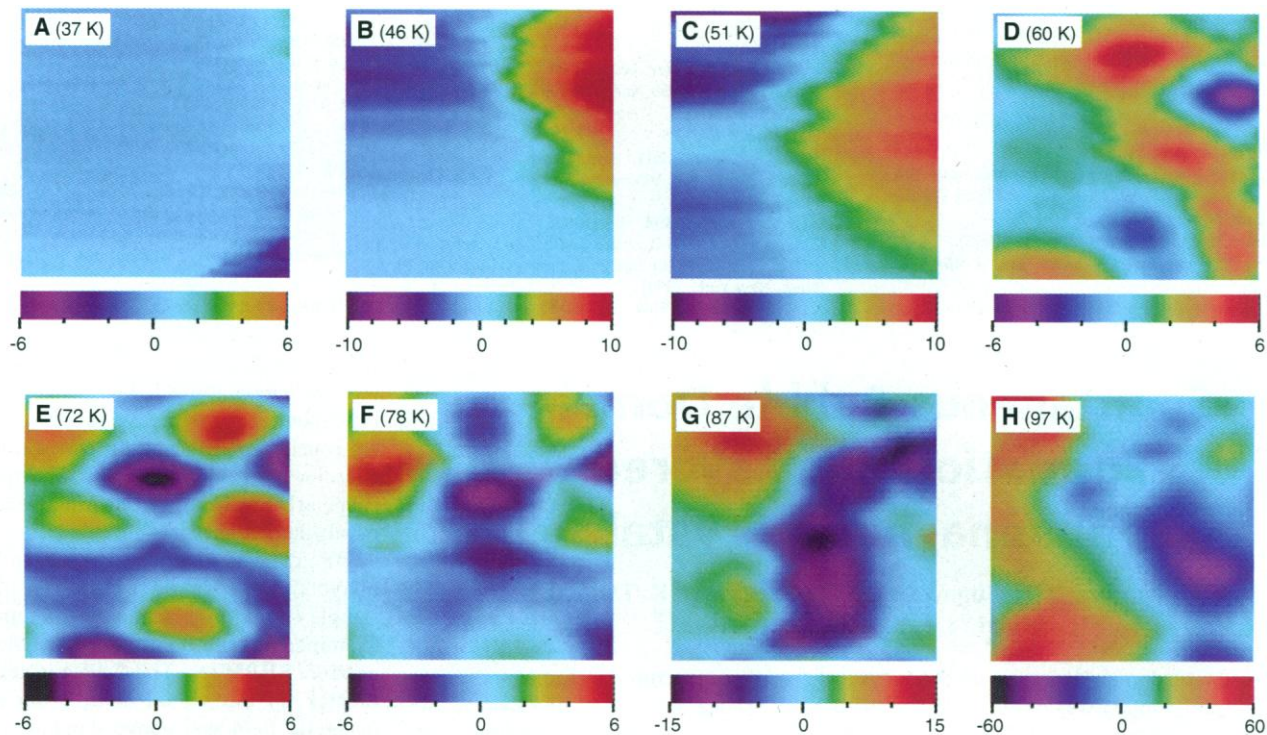


Fig. 1. Variation of the domain structure in the cleaved surface of a $\text{La}_{1.4}\text{Sr}_{1.6}\text{Mn}_2\text{O}_7$ single crystal. Color bars indicate the measured magnetic field (in milliteslas) normal to the sample surface. Scanned areas of all panels are $8\ \mu\text{m}$ by $8\ \mu\text{m}$. Temperatures: (A) 37 K, (B) 46 K, (C) 51 K, (D) 60 K, (E) 72 K, (F) 78 K, (G) 87 K, and (H), 97 K. (I), (J), and (K) are the same as (B), (E), and (H) but sharing the same color scale.

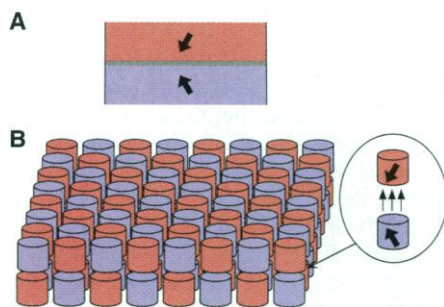


Fig. 2. Schematic of the magnetic structure. (A) Arrangement of the magnetization along the c axis. The c -axis components of the magnetization are opposite each other. The domain boundary corresponds to a nonmagnetic layer. (B) A domain structure consisting of spontaneously formed bubble domains at 72 K. The c -axis component of the magnetization of each domain is alternately arranged. Inset shows that the upper bubble domain is supplied with a magnetic field from the lower magnetic domain adjacent along the c axis. Thick and thin arrows represent the magnetization and the magnetic field lines, respectively.

anged irregularly. At 72 K, the domains became circular and uniform-sized in a close-packed array (Fig. 1E). As the temperature was increased further, the circular domains began to collapse again into an irregular B_z pattern at 78 K (Fig. 1F). Such a remarkable change in domain structure with temperature was not seen in the cubic $\text{La}_{0.65}\text{Ca}_{0.35}\text{MnO}_3$ film reported earlier (9). Domains with a typical stripe shape were not observed in the present experiment, although they are commonly observed in other ferromagnetic materials in zero magnetic field. Figure 1E shows the spontaneous formation of a bubble domain without an external magnetic field.

The measured B_z is much smaller than that expected if the thickness of the domain is comparable to the sample thickness. This can be explained by assuming that the domain stacks along the c axis with the c -axis component of magnetization opposite that of the adjacent domain (Fig. 2A). Therefore, the domain is supplied a magnetic field from the

adjacent domain, as these domains repel each other.

This situation is similar to that in which a bubble domain is formed in a ferromagnetic material by applying an external magnetic field. For the stable formation of the bubble domain, the condition $H_B + H_W = H_D$ is required, where H_B , H_W , and H_D are the bias magnetic field from the adjacent domain, the magnetic field originating from the domain wall, and the demagnetization field of the bubble domain, respectively (1). H_B , H_W , and H_D are functions of the bubble diameter d , the domain thickness t , and the saturation magnetization M_S (10). The stable bubble diameter calculated from the above condition by adopting t , as evaluated from the measured B_z and the c -axis component of M_S ($\equiv M_C$) [see figure 1b of (5)], is approximately the same as the observed diameter shown in Fig. 1E.

The variance in the domain structure as a function of temperature (Fig. 1, D to F) is

attributed to the change in the magnetostatic energy of the domain caused by the relation of the temperature-dependent M_C to the stability of the formation of the bubble domain (I). The elongated domain is transformed into the collapse of the bubble domain as M_C is decreased (Fig. 1, D and F), because H_W increases and H_D decreases with decreased M_C , leading to the instability of the domain as a result of decreasing magnetostatic energy. For the formation of the bubble domain at 72 K, the important factor is not only the value of M_C but also the thin domain originating in the large anisotropic crystalline structure. If the domain is thicker, the elongated domain will appear because H_D increases with increasing t . The balance between the appropriate value of M_C and the thickness of the domain is preserved for the stable formation of the bubble domain at 72 K.

At 87 K, a steep structure appears with a larger absolute value of B_z than that at lower temperatures (Fig. 1G). In this temperature range, the magnetic moments nearly lie in the MnO_2 plane. Therefore, the structure represents a stray field arising from the boundaries of magnetic domains with in-plane magnetization. At 97 K, the B_z value of the observed structure is increased because of further tilting of the magnetic moments toward the MnO_2 plane (Fig. 1H). The size of the domain is nonuniform.

The observed close-packed bubble domain in the structure is promising for high-density magnetic recording. Removing the need for an external magnetic field for the generation of the domain provides a cost incentive for the downsizing of the device. In terms of its practical application, the bubble domain structure obtained in this study is still limited in temperature range; moreover, the size of the domain is not small enough. Further optimization of the material should be achieved through raising the temperature of the stable formation of the smaller bubble domains, either by finding a new composition for the layered structure or by fabricating an artificial layer structure.

References and Notes

1. A. H. Bobeck and E. Della Torre, *Magnetic Bubbles* (North-Holland, Amsterdam, 1975).
2. C. Kittel, *Rev. Mod. Phys.* **21**, 541 (1949); B. Kaplan and G. A. Gehring, *J. Mag. Mag. Mat.* **128**, 111 (1993).
3. Y. Moritomo, A. Asamitsu, H. Kuwahara, Y. Tokura, *Nature* **380**, 141 (1996).
4. T. Kimura *et al.*, *Science* **274**, 1698 (1996).
5. T. Kimura, A. Asamitsu, Y. Tomioka, Y. Tokura, *Phys. Rev. Lett.* **79**, 3720 (1997).
6. R. H. Heffner *et al.*, *ibid.* **81**, 1706 (1998).
7. T. G. Perring, G. Aeppli, T. Kimura, Y. Tokura, M. A. Adams, *Phys. Rev. B* **58**, R14693 (1998).
8. T. Fukumura, thesis, University of Tokyo (1998).
9. Q. Lu, C.-C. Chen, A. de Lozanne, *Science* **276**, 2006 (1997).
10. H_W and H_D are defined as follows:

$$H_W = \sigma_w / (dM_s)$$

where σ_w is domain wall energy per unit area.

$$H_D = 8M_s(1 + d^2/t^2)^{1/2} E(k, \pi/2) - 8dM_s/t$$

where

$$E(k, \pi/2) = \int_0^{\pi/2} (1 - k^2 \cos^2 \theta)^{1/2} d\theta$$

and $k = (1 + t^2/d^2)^{-1/2}$. H_B is given by the magnetic field from the rectangular parallelepiped magnet with magnetization of M_s and dimension of $d \times d \times t$.

11. Supported by Core Research for Evolutional Science and Technology (CREST) of the Japan Science and Technology Corporation (JST) and by The New Energy and Industrial Technology Development Organization (NEDO), Japan.

11 March 1999; accepted 11 May 1999

Century-Scale Shifts in Early Holocene Atmospheric CO₂ Concentration

Friederike Wagner,¹ Sjoerd J. P. Bohncke,² David L. Dilcher,³ Wolfram M. Kürschner,¹ Bas van Geel,⁴ Henk Visscher¹

The inverse relation between atmospheric carbon dioxide concentration and stomatal frequency in tree leaves provides an accurate method for detecting and quantifying century-scale carbon dioxide fluctuations. Stomatal frequency signatures of fossil birch leaves reflect an abrupt carbon dioxide increase at the beginning of the Holocene. A succeeding carbon dioxide decline matches the Preboreal Oscillation, a 150-year cooling pulse that occurred about 300 years after the onset of the Holocene. In contrast to conventional ice core estimates of 270 to 280 parts per million by volume (ppmv), the stomatal frequency signal suggests that early Holocene carbon dioxide concentrations were well above 300 ppmv.

The records of the relation of greenhouse gases to Quaternary climate change come largely from ice cores from Antarctica and Greenland. Trends in the atmospheric CO₂ amount parallel those of the temperature inferred from the isotopic compositions of oxygen ($\delta^{18}O$) and hydrogen (δD) during the past 250,000 years, showing that variation in greenhouse gas concentrations is an important factor in long-term glacial-interglacial climate evolution (*1*). Carbon dioxide data from ice cores also seem to correlate with millennial-scale temperature changes (*2*). However, a correlation of atmospheric CO₂ amounts to century-scale climate shifts in the Holocene (*3, 4*) is still unclear. Most of the Holocene ice core records from Antarctica do not have adequate temporal resolution (*5*). In Greenland ice, the Holocene CO₂ concentrations are generally considered to be influenced by postdepositional enrichment (*6*). Because of the apparent inadequacies and controversies in the CO₂ records derived from ice sheets, alternative methods have to be developed to improve the accuracy of detecting and

quantifying possible short-term shifts in the Holocene atmospheric CO₂ regime. Here, we provide a century-scale record of early Holocene atmospheric CO₂ amounts, based on a stomatal frequency analysis of leaves that were buried in peat deposits.

An analysis of herbarium material collected over the past 200 years and controlled growth experiments under preindustrial CO₂ amounts (*7, 8*) has shown that, for Northern Hemisphere tree species, stomatal frequency decreases linearly as atmospheric CO₂ concentration increases. A near-annual analysis of a 40-year record of the buried leaves of a solitary growing birch (*Betula pendula*) has illustrated that deciduous trees are equipped with a plastic phenotype, capable of a lifetime adjustment of stomatal frequency to an increase in anthropogenic CO₂ (*9*).

Stomatal frequency is conventionally expressed in terms of stomatal density and stomatal index (SI) (*10*). In contrast to stomatal density, SI expresses frequency changes independently of variation in epidermal cell size and therefore is the more sensitive parameter for detecting stomatal frequency response to changes in CO₂ concentration (*11*). The effects of intrinsic variation in SI values within and among leaves of an individual tree species (*11, 12*) can be accounted for analytically, allowing the replication of temporal trends of mean SI values (*9, 13*). At least for European tree birches (*B. pendula* and *B. pubescens*), field studies and controlled-envi-

¹Laboratory of Palaeobotany and Palynology, Utrecht University, Budapestlaan 4, 3584 CD Utrecht, Netherlands. ²Netherlands Centre for Geo-ecological Research, Faculty of Earth Sciences, Free University, De Boelelaan 1085, 1081 HV Amsterdam, Netherlands. ³Paleobotany Laboratory, Florida Museum of Natural History, University of Florida, Gainesville, FL 32611, USA. ⁴Netherlands Centre for Geo-ecological Research, Department of Palynology and Paleo/Actuocology, University of Amsterdam, Kruislaan 318, 1098 SM Amsterdam, Netherlands.